LAWRENCE
LIVERMORE
NATIONAL
LABORATORY

LLNL-TR-817426

Evaluation of Ceramic Heat Exchanger for Next-Generation Concentrated Solar Power

C. Santa Lucia

December 7, 2020

Disclaimer

This work performed under the auspices of the U.S. Department of Energy by Lawrence Livermore National Laboratory under Contract DE-AC52-07NA27344.

Lawrence Livermore National Laboratory

Evaluation of Ceramic Heat Exchanger for Next-Generation Concentrated Solar Power

Christina Santa Lucia
Summer Internship

August 21, 2020

Disclaimer

Acknowledgements

Funding for this report was provided by NNSA Minority Educational Institution Partnership Program and this material is based upon work supported by the U.S. Department of Energy's Office of Energy Efficiency and Renewable Energy (EERE) under the Solar Energy Technologies Office Award Number 35929. The U.S. Department of Energy Solar Energy Technologies Office supports early-stage development to improve affordability, reliability, and performance of solar technologies on the grid. Learn more at http://energy.gov/solar-office.

Table of Contents

1 Summary

The U.S. Department of Energy has identified a third generation of concentrated solar power (Gen3 CSP) technologies to minimize cost of CSP produced electricity. By developing these technologies further, it is forecasted that Gen3 CSP will meet the levelized cost of electricity (LCOE) SunShot target of 6 cents/kWh to compete with dominant, conventional non-renewable energy sources (1). The focus for advancing CSP systems for Gen3 is to increase overall system efficiency. Thus, reevaluating second-generation systems, superheated steam-turbine power cycles, and implementing more advanced power cycles is essential. Specifically, it has been identified that a supercritical carbon dioxide (sCO_2) Brayton cycle can increase the net thermal-to-electric efficiency to over 50% for CSP power tower configurations (2). Compared to conventional superheated steam Rankine cycle systems, more extreme operating conditions are required and pose critical barriers to overcome in the field of materials and manufacturing for Gen3 CSP.

To move towards a more efficient system, the overall system temperatures must be increased compared to the second generation systems by over 200°C. Past studies indicate that conventional steam Rankine systems can be replaced with sCO2 Brayton cycles, raising the temperature from about 600 to 800°C and increasing the efficiency to over 50%. With higher efficiencies the overall size, complexity, and thus cost of turbomachinery components are decreased (3). To implement this system, salt chemistry and heat exchanger technologies need to be addressed when considering the liquid media pathway.

Molten-salt chemistry is essential to reassess when implementing a sCO_2 cycle when considering the liquid media pathway. Currently, in molten-salt power tower configurations the working fluid is a blend of sodium and potassium nitrate with a limit of thermal stability around 600°C. Alternative salts such as chloride or carbonate salt blends have been identified to provide a much higher limit of thermal stability to be able to perform at higher temperatures up to 750/800°C. These salts must also exhibit favorable heat transfer and energy storage properties: low melting point with high heat capacity and high thermal conductivity. Low corrosion behavior is also important for the longevity of system components. Additionally, cost must be taken into consideration.

Implementing a sCO_2 Brayton power cycle also requires advanced heat exchangers. Current heat exchangers used in the Rankine power cycle are limited. The introduction of chloride salts, for example, requires alternative heat exchangers that can withstand temperatures up to about 800°C without being excessively corroded over the lifetime of the power plant. The exploration of materials, design, and manufacturability of the heat exchanger is believed to be a key component to the success of Gen3 CSP systems based on the liquid media pathway. Two dominating factors for the heat exchanger material are the ability to resist salt corrosion and maintain required strength at nominal operating temperatures and over the desired lifetime. Several other criteria must also be evaluated for successful implementation including ideal mechanical, thermal and chemical properties. Specifically, assessments of strength, fatigue, thermal expansion, and thermal conductivity are crucial for its success. It is also vital to take into consideration manufacturability and cost for reaching the SunShot CSP LCOE goal.

2 Concentrated Solar Power

Concentrated solar power technologies implement mirrors to concentrate sunlight to a central receiver at the top of a power tower. Within the receiver is a molten salt that collects the heat from the sunlight. The thermal energy is then exchanged to the working fluid of the power cycle to drive a turbine-generator to create electricity. However, current systems have high costs that lead to commercial barriers. The Department of Energy's Gen3 CSP plans seek to increase the efficiency while reducing power plant size and cost for the future of CSP (1).

The Energy Department put out the 2012 SunShot Vision Study to show that reaching a levelized cost of energy of 6 cents per kWh will become cost competitive with other technologies and can lead to more significant deployment in the U.S. The U.S. Department of Energy's Solar Energy Technology Office (SETO) has identified that implementing Brayton power cycle and improving energy efficiency by raising the operating temperatures will reduce the cost of the overall system. SETO has identified key technical gaps to be addressed and their challenges through their Multi-Year Program Plan for FY 2018-2022 (2).

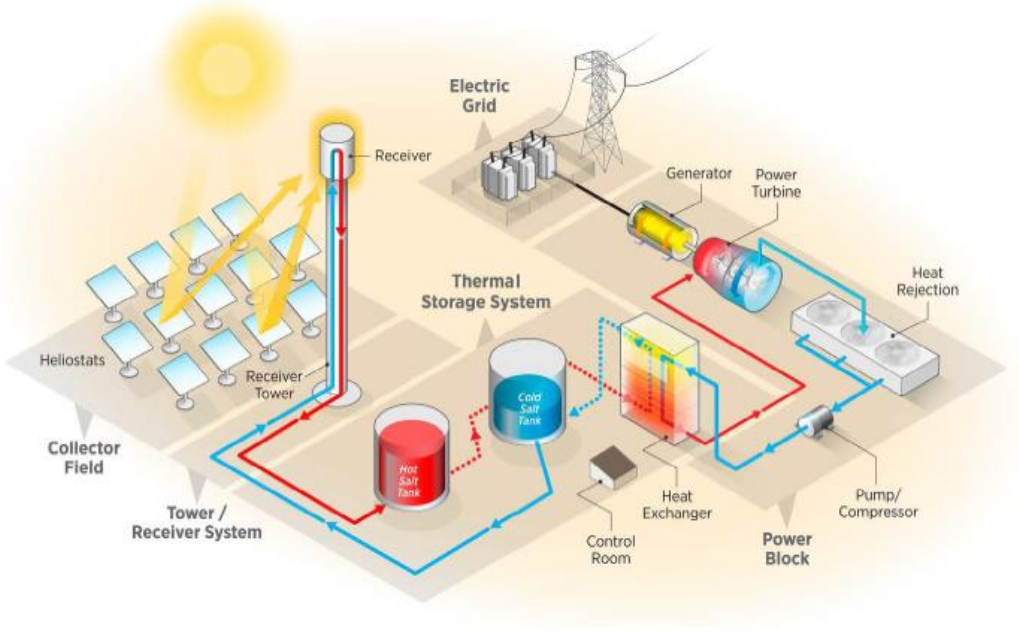

Figure 1. Molten-salt power tower configuration, with thermal storage. Within the heat exchanger, there is a transfer of thermal energy from molten salt to sCO_2. The power block represents the closed sCO_2 loop. (1)

To help the concentrated solar industry resolve key barriers in CSP's technical innovation, four distinct objectives are outlined to break down the overarching goal of technical advancement. Two of the four are tied to directly increasing the operating temperatures and reducing the size and cost of the thermal systems and are the focus of this evaluation. The SETO outlines the plans, challenges, and goals to achieve: 1. Higher operating temperature and 2. Smaller power plant scale.

2.1 Higher Operating Temperature

The purpose of this objective is to reach a direct solar illumination to AC power efficiency for a dry-cooled CSP plant of over 30%. The plan is to have the heat transfer fluid's temperature reach over 700 °C. Currently, the operating temperature of a conventional CSP plant is limited by the thermal stability of the nitrate-based molten-salt heat transfer fluid, which has a limit of under 600°C. To operate at higher temperatures, new materials must be investigated to determine a thermally and chemically compatible alternative. One of the three heat transfer media pathways identified by the Gen3 Roadmap is to use a liquid. Thus, replacing the conventional molten salt with a high-temperature alternative. Solid and gas phase heat transfer media are also under consideration and would be a fundamental change compared to Gen2 systems.

2.2 Smaller Power Plant Scale

The goal of this objective is to create a supercritical $10MW_{ac}$ power cycle converting energy of the working fluid into an alternating current with a minimum efficiency of 50%. The plan is to develop a sCO_2 Brayton power cycle for the power plant. For this to be effective, the materials of the current heat exchanger must be reevaluated to be compatible with a new molten-salt-sCO_2 heat exchange and with higher ramp rates and dry cooling. However, the main challenge is that this has not been demonstrated in a commercial application.

3 Heat Exchangers

3.1 Shell-and-Tube Heat Exchangers

The most common type of heat exchanger, shell-and-tube, consists of set or bundle of tubes contained within a container or shell. The tubeside fluid flows within the tubes, and usually is the fluid at higher pressure. The shellside fluid flows around these tubes. The heat from the hot fluid flows through the heat exchanger material to raise the temperature of the cold fluid. Some exchangers have baffles within the shell that are used to increase the heat transfer rate between the two fluids by increasing turbulence of the flow. If leaking is a high-risk issue double walled tubes can also be utilized to reduce leaking into the shellside fluids. Other modifications for optimizing heat exchanger properties include introducing finned tubes and adjusting the construction and shaping of the tubes. The Tubular Exchanger Manufacturers Association outlines many shell-and-tube heat exchanger construction standards and designations for various types (4).

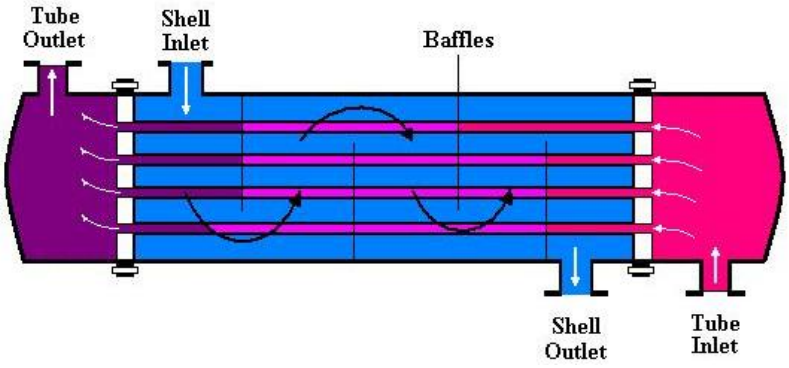

Figure 2. Diagram of shell-and-tube heat exchanger. (5)

3.2 Plate-Type Heat Exchangers

Plate-type heat exchangers use several stacks of “plates” that the working fluids flow through with alternating gaskets, other seals, or direct bonding. One heat transfer fluid can flow through every second pair of plates, whereas the other flows through the opposite pairs, creating a stack of alternating fluids flowing in opposite directions. This allows for a large surface area for the heat transfer to take place, making these exchangers highly effective. Like the shell-and-tube exchangers, turbulence is introduced to increase the heat transfer rate even further by creating corrugations in each plate. These are commonly in a herringbone pattern. Compact heat exchangers with high efficiency can be made by having the two fluids flow through microchannels between the plates. In this case, both fluids are flowing in between every plate, but in separate microchannel domains with heat exchanged across the thin walls separating those domains.

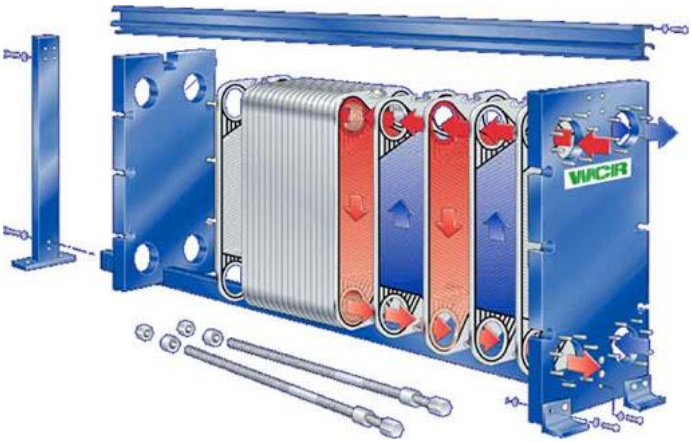

Figure 3. Drawing of plate-type heat exchanger showing alternating flow. (6)

3.3 Air-Cooled Heat Exchangers

Instead of transferring heat between two closed fluid systems, air-cooled heat exchangers blow cool air to act as one of the heat transfer liquids. In this style, the configuration consists of a bank of finned tubes with a fan. The two main types are forced or induced draft heat exchangers and are dependent on the location of the fan within the bank at either the top or bottom, respectively. The fins can also take on various shapes depending on the required properties of the heat exchanger (7,8).

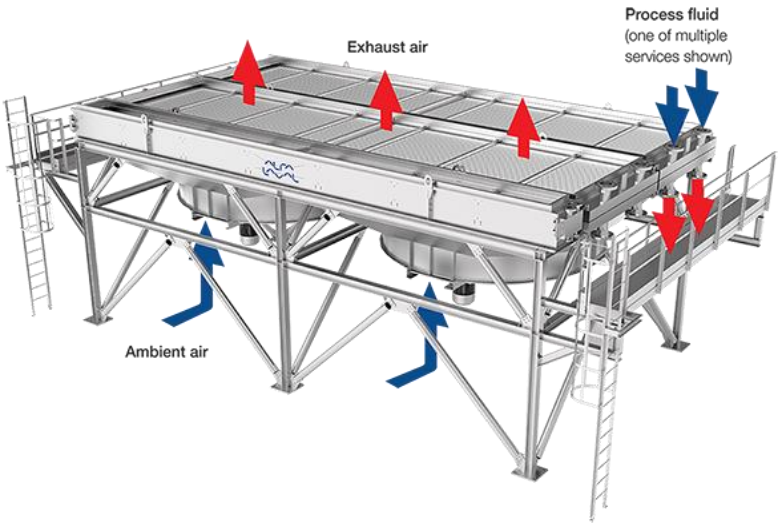

Figure 4. Schematic of flow within industrial air-cooled HEX. (9)

4 Heat Transfer through Triply Periodic Minimal Surfaces

Triply periodic minimal surfaces (TPMS) are 3-D geometries present in a number of natural structures (10,11). Creating these structures had been previously inaccessible with conventional forming methods and machining techniques. Developments in additive manufacturing enable their creation and further could allow a vast array of structures to be realized (12–14). By adjusting the properties of these structures, TPMS can potentially be utilized in a vast array of applications. TPMS structures are of great interest to the fields of mass and heat transfer due to its curved and twisted hollow channels which have exhibited enhanced heat and mass transport (15–22).

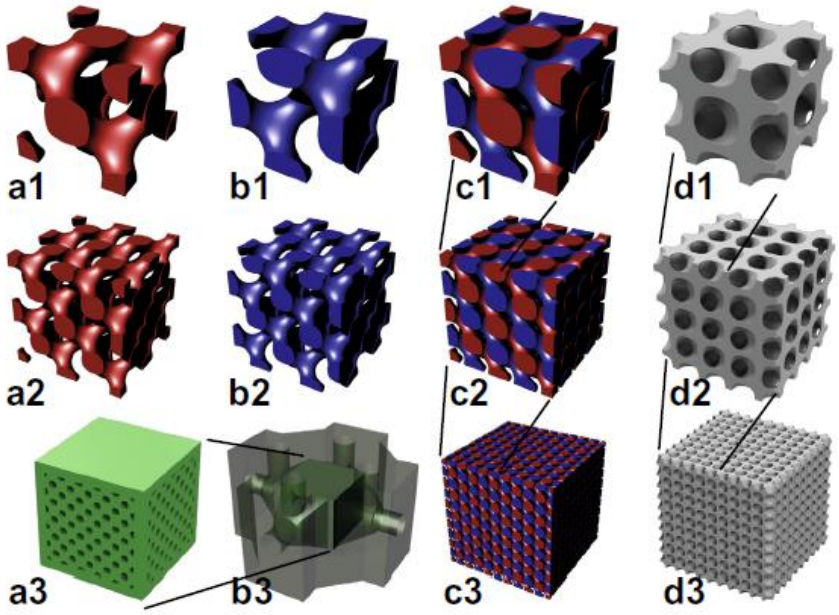

Figure 5. Schwarz-D TPMS. (a1, b1) individual volume domains within unit cell, (a2, b2) volumes within 2x2 unit cell, (c1, c2, c3) interweaving volumes are shown, with increasing dimensions, (d1, d2, d3) Schwarz-D TPMS structure with increasing dimensions. (a3) example of printed TPMS structure, (b3) potential configuration of TPMS structure in a HEX structure. (23)

Specifically, TPMS structures have been of interest when creating novel, high-performance heat exchangers. TPMS geometries contain two interweaving volume-domains separated by a wall (24). When each of the microchannels contain a working fluid and there is a temperature differential between them, heat conduction occurs through the structure walls. These microchannels twist and extend in all directions leading to further increased mixing and thus a high heat transfer rate (23). Other properties affecting the transfer rate include wall thickness, cell size, and structure geometry. Heat exchange is also affected by the thermal conductivity of the structure's material. Different materials can be implemented to allow for a wide range of operating temperatures.

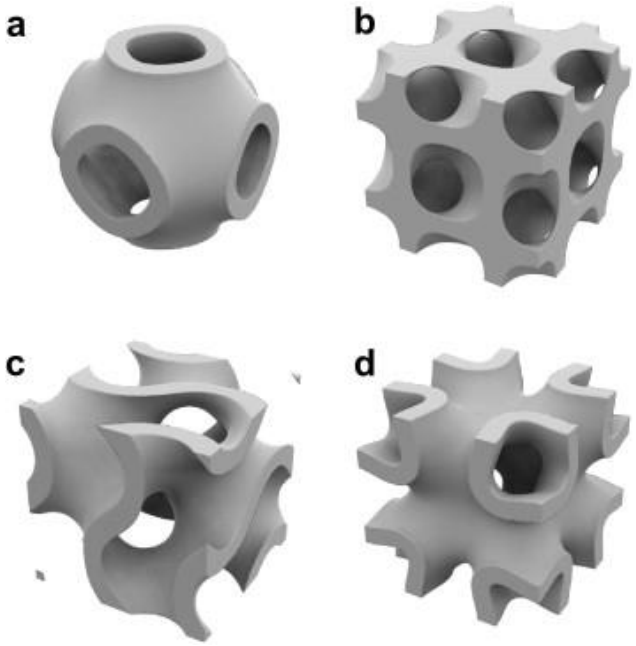

Figure 6. TPMS structures. (a) Schwarz-P, (b) Schwarz-D, (c) Schoen-G, (d) IWP. (23)

Femmer et al. highlights four specific TPMS geometries as promising contenders for effective heat and mass transport: Schwarz-D, Schwarz-P, Schoen-G, and IWP, shown in fig. 6 (24,25). Using 3-D rapid prototyped 5x5 unit cell membranes, estimates are made for the geometries to rank their structure-dependent performance. Essentially, it is concluded that the estimates for *all* geometries outperform conventional tube and flat plate heat exchangers (23). Further, with respect to the dimensionless Reynold's number, the Schwarz-D membrane exhibits the greatest heat transfer. Additionally, with increasing Reynold's number, Schwarz-D performs best with varying ratios of friction to heat transfer by being the closest to a constant value. Therefore, Schwarz-D is an excellent candidate for TPMS heat exchangers.

5 Ceramic Heat Exchangers

For Gen3 CSP heat exchangers to be successful, the use of conventional heat exchanger materials must be revisited. It is unclear if the materials can successfully perform at the high temperatures for proper molten-salt-sCO_2 heat exchange. Developments in ceramics and ceramic composites show great promise to efficiently transfer heat in such an extreme environment. The properties of some of ceramic materials are extremely attractive for heat exchangers.

Generally, ceramics have high use temperatures, up to 1200°C or higher, whereas carbon steel and stainless steel can only withstand operating temperatures of 425 or 650°C, respectively. For extremely aggressive chemical environments, ceramics have high resistance to chemical effects and corrosion (26). However, it also has inherent limitations with its material properties. Ceramics are brittle and fail catastrophically without much warning. By fracturing without reaching plastic deformation, ceramics have low toughness. Additionally, porosity of ceramic materials further degrades properties, due to pores acting as stress concentrators within the material. Though monolithic ceramics have a few positive characteristics, there are clear limitations. With additional treatment, this hard, porous, brittle material's properties can be modified by utilizing it within a composite.

Ceramic composites, such as ceramic matrix composites (CMSs), are a mix of two or more materials to improve desired properties (27). CMCs consist of two parts: a matrix and a reinforcement material. The matrix is the main material that is present in greater quantity and the reinforcement acts to enhance or reinforce the properties of the matrix (28). Combining these makes it possible to create materials not only with high-temperature stability and corrosion resistance, but higher toughness, strength, and thermal shock resistance. Specific composites can be chosen for their top-performing qualities with less limitations than monolithic ceramics, depending mainly on the intended application (29). Essentially, CMCs' versatile nature allow them to be utilized in a variety of conditions for a potentially wide number of fields.

5.1 Examples from Literature

Caccia et al. successfully demonstrates a ZrC/W-based composite printed-circuit type heat exchanger strongly outperforming a conventional nickel-alloy HEX at a lower cost (30). For material selection, ZrC/W was chosen for its promising high-temperature thermal, mechanical, and chemical properties and the cost-effective nature of its production. At ~750°C, this CMC has a failure strength of over 350 MPa, allowing the HEX to operate at a power density 2 times that of stainless steels or Ni-alloys, shown in fig 7. It also exhibits a thermal conductivity 2-3 times higher than conventional heat exchanger metals, all at a lower cost.

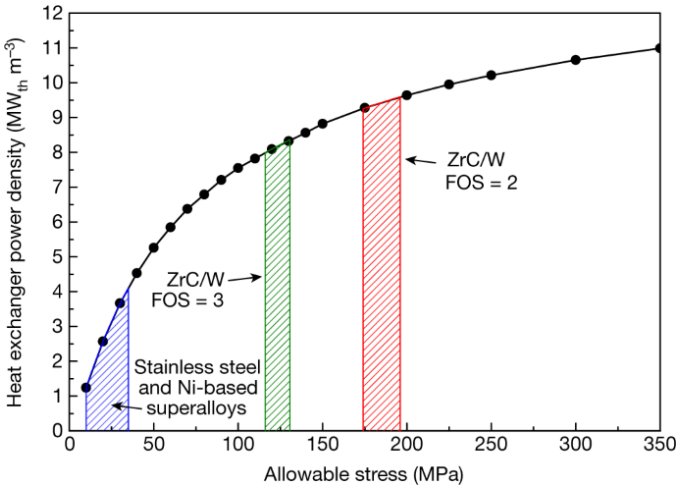

Figure 7. Calculated power density vs allowable stress of stainless steel, nickel-based superalloy, and ZrC/W printed circuit heat exchanger at ~750°C. (30)

Haunstetter et al. investigated a SSiC ceramic microchannel plate-type heat exchanger, seen in fig. 8, under both high temperature and pressure conditions (31). Using air as a heat transfer fluid, a temperature of 800°C and pressure of 0.5 MPa was applied and an effectiveness of 0.94 to 0.97 was achieved. Results of this experiment proved the stability of this ceramic HEX under the high temperature/pressure conditions. Previously, ceramic heat exchanger investigations included computer simulation or testing under one of the two extreme conditions, whereas this research investigated performance under actual conditions.

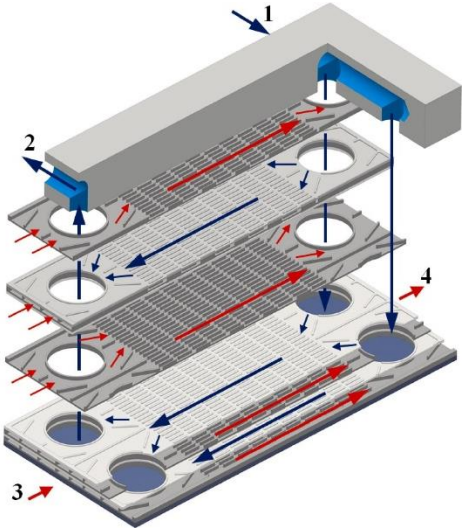

Figure 8. Schematic drawing of fluid streams within SSiC plate-type heat exchanger. (1) gas input, (2) gas output, (3) flue input, (4) flue output. (31)

6 Ultra-High Temperature Ceramics and Related Materials

Ultra-high temperature ceramics (UHTCs) are attractive for implementation in extreme environments due to their special properties of high thermal conductivity, strength, and melting temperature while having the ability to survive in extremely high temperature and pressure environments. The first investigations of UHTCs were mainly for use in the aerospace industry. NASA had identified this material as a candidate for aerospace vehicles due to their exposure to extreme temperatures and a chemically aggressive environment. Most of the early research of UHTCs were government funded and published as NASA technical notes, which can be found in the NASA Technical Reports Server (NTRS) (32–35). As the properties of these materials were identified, specific routes for its use included hypersonic vehicles and vehicles that experience atmospheric reentry (35,36). Following this, UHTC's applications have expanded to a diversity of fields and are broadening still (37). For the future of concentrated solar power, UHTCs have a high potential for use in the supercritical Brayton cycle heat exchanger, where temperatures can exceed the performance limits of conventional metallic materials. This is made apparent by the ZrC/W heat exchanger described in the previous section.

Figure 9. Image of NASA Space Shuttle, application of a thermal protection system based on ceramic and glass materials. (38)

7 Materials Evaluations

For this potential application, several UHTCs and related materials of group IV-VI transition metal borides, carbides, nitrides, and silicides are investigated. Each is given a Figure of Merit (FOM) value to determine the most promising materials based on seven key ranking factors and, following evaluation, each material is ranked based on this value. The FOM factors include thermodynamic stability assessment based on Ellingham diagrams, thermodynamic stability assessment based on molten salt synthesis, processing assessment based on pressureless sintering, cost assessment based on raw materials costs, availability assessment based on the availability of bulk raw materials and test materials, mechanical properties assessment based on elastic modulus, and thermal properties assessment based on thermal conductivity. Further, top materials are determined with highest FOM, the sum of all factor scores for each material to down select eight materials for testing.

7.1 Thermodynamic Stability Assessment based on Ellingham Diagrams

Ellingham Diagrams for each material can be utilized to find each of their thermal stabilities at 1100 K. This is quantified by summing the Gibbs free energy from negative and positive elemental interactions of the UHTCs, salt components, and impurities. The sum is then subtracted by 500 and then divided by 350 to provide a number between 0 and 1. The value is then rounded to the nearest tenth. If information could not be found, the value is 0.

7.2 Thermodynamic stability assessment based on Molten Salt Synthesis

This parameter focuses on demonstrating successful past molten salt synthesis through document searches, with intermediate levels determined using background knowledge. A search of each compound name and “molten salt synthesis” was conducted using the Web of Science database. The level of documentation was then quantified with values from 0 to 1. To receive a 1, the UHTC must have published data on its successful molten salt synthesis. A value of 0.8 is given if the molten salt synthesis of the compound is confirmed but has unpublished results. Next, a compound is given a score of 0.5 for probability for success where the compound is intermediate between two validated successful compounds. Where the compound is intermediate between one validated and another compound with high probability, a score of 0.3 is given. A score of 0 is for insufficient data for the compound.

7.2.1 Demonstration of Factor B – Molten Salt Synthesis

The score for this factor is determined by conducting a Web of Science database search of the compound name and “molten salt synthesis”. Here, we provide a sampling of this documentation with some parameters of interest: type of salt, temperature of reaction, and environment for its synthesis. The examples address one boride, carbide, nitride, and silicide as a group V compound.

First, vanadium boride was found to be synthesized with sodium chloride, at temperatures of 850-1000 °C (39). Niobium carbide uses calcium chloride with an ideal temperature of 900 °C in air (40). Vanadium nitride is formed in potassium chloride at temperatures 600 to 1000 °C (41). Lastly, vanadium disilicide is synthesized with molten magnesium chloride at a temperature of 650 °C in an autoclave (42). With each of these examples, it is exhibited that a Web of Science database search, documentation of molten-salt synthesis of various compounds can be

found. The synthesis of these materials in molten chloride salts at high temperature implies stability, otherwise the high surface area materials would readily degrade.

7.3 Processing assessment based on Pressureless Sintering

The prior method is used for searching for demonstration of pressureless sintering with a Web of Science database search of the compound and "pressureless sintering". It is essential to confirm that with pressureless sintering, the compound has closed porosity with 92-96% theoretical compound density (%TD) to be able to effectively follow with hot isostatic pressing to achieve full density and achieve optimum properties. The lowest and highest quantitative levels of documentation are also similar, with differing intermediate values. With documentation of reaching %TD between the desired range, the UHTC receives a 1. Intermediate candidates between two validated compounds that reach 92-96%TD receive a score of 0.8. If the material is intermediate between one validated and the other a high likely compound, it receives a 0.5. If data is insufficient, the compound receives a score of 0.

7.3.1 Demonstration of Factor C – Pressureless Sintering

The search for demonstrations of pressureless sintering is similar to the prior search, however the motivation is slightly different. Searching for demonstrations of various compounds shows that with pressureless sintering, a closed porosity is reached. If a density of 92-96%TD is not reached hot isostatic pressing, the next process, will not be effective. While searching, parameters for pressureless synthesis were recorded such as %TD, atmosphere, temperature, ramp rate, and length of time. These examples follow the previous, with one boride, carbide, nitride, and silicide group V compounds.

Vanadium boride in SiC with pressureless sintering reaches a 97%TD when at 2150 °C for 1 hour in a vacuum (43). However, the composite is not representative of the pure material or at least a composite that is primarily made up of the UHTC material and so this paper would be disqualified from the analysis. Next, tantalum carbide was able to reach 92-96.7%TD in an argon atmosphere in a graphite reactor at 1400 °C for 1 hour and is a successful demonstration (44). Niobium nitride was classified as fully dense with closed porosity when in a graphite reactor at 1130 °C with a ramp rate of 100 °C/min (45). However, this result was obtained using pressure-assisted sintering technology and would be disqualified from the analysis. Lastly, niobium/niobium silicide composites reached 99.17%TD when sintered at 1500 °C for 10 minutes (46). However, the composite was primarily metallic niobium and was consolidated with pressure-assisted sintering technology and would be disqualified from the analysis.

7.4 Cost Assessment based on Raw Materials Cost

A cost assessment is always essential when considering implementation of a new material. Estimations of bulk powder prices are from bulk suppliers or estimated from a correlation developed from cost comparisons between bulk and small scale quantity suppliers with an emphasis on suppliers with openly published prices. Bulk prices are found from nine suppliers. The grading values are determined by the price of the candidate with respect to an estimated price of Haynes 230, a potential nickel superalloy candidate material. A score of 1 is given if the compound by volume has a lower cost than the Haynes 230 estimate. If a thermal conductivity factor is used to compare the two prices, and it is lower than Haynes 230, the score is 0.7. If the cost is lower than Haynes 230 estimate when using thermal conductivity and an

emissivity factor, it receives 0.3. Candidate prices exceeding Haynes 230 estimate even with additional factors taken into consideration, then they are scored a 0.

7.5 Availability assessment based on Bulk Raw Materials and Test Materials

An internet search is conducted to determine the published availability of bulk powder and the ability to test samples from a commercial supplier. For quantitative evaluation, if both bulk powder and test samples are published for the compound, it receives a 1. If only the test sample price is published, the candidate's score is 0.5. Lastly, if the test samples are available but without published prices, a score of 0.3 is given.

7.6 Mechanical properties assessment based on Elastic Modulus

The elastic modulus of a material is a quantity that describes a material's performance under an applied stress and is loosely correlated to strength without having the scatter that is common in strength data due to the dependence on processing history. Published elastic modulus values from the Materials Project are used. Assuming typical Ashby Plot results: the elastic modulus directly relates to the strength of the material. Each candidate's evaluation score is determined by its modulus value level: if 200-299 MPa, 300-399 MPa, 400-499 MPa, 500-599 MPa, and 600+ MPa, the scoring is 0.2, 0.4, 0.6, 0.8, and 1.

7.7 Thermal properties assessment based on Thermal Conductivity

Using two comparable data sources with a range of materials or sources, the thermal conductivity for each UHTC is found. The grades are distributed based on each value. If greater than 20 W/mK, the compound receives a 1. A thermal conductivity 10-20 W/mK is given a score of 0.7. If between 8-10 W/mK, the candidate receives a score of 0.3. Lastly, if the thermal conductivity is lower 8 W/mK or data cannot be found, the UHTC receives a score of 0.

8 Ceramic Additive Manufacturing

ASTM International defines additive manufacturing as building objects layer-by-layer utilizing computer-aided design. This includes the use of 3D models created directly with computer-aided design (CAD) software or imported from computer tomography (CT) scanning (47). With this manufacturing process, the model is then loaded into a machine which can build layers of the material to form the object. Due to this, additive manufacturing (AM) greatly varies from traditional manufacturing methods that cut, grind, and drill away excess material from one solid, larger piece. AM has been recognized by many engineering groups and societies as an extremely fast-growing technology with extremely high potential. In 2009, ASTM International formed a small committee for additive manufacturing technologies, which has now broadened to over 600 members representing 25+ nations, leading to 14 internationally recognized technical standards for AM. The recognized potential for AM in several fields continues to grow. In 2020, ASTM International launched an Additive Manufacturing Center of Excellence focusing specifically on the research and development of future AM standards and supports research partnerships with universities, private companies, and government organizations. This technology has simply unprecedented capabilities, and its potential is internationally recognized.

Additive manufacturing goes beyond what was previously possible with conventional and expensive machining. The ability to create unprecedented parts, decrease lengthy time spans of prototyping, and significantly reduce manufacturing costs at low production volumes are the three main advantages of this technology. The utilization of CAD plays a large role in creating a variety of novel complex geometries. Even objects with unknown dimensions such as living forms can be imported into CAD software using scanning techniques to create a printable 3D model. Additionally, these models can be easily used for shape optimization. AM also plays a large role in changing the prototyping process by significantly increasing the speed of the creation of prototyping over conventional methods. This further reduces the overall timespan of the development and implementation of parts, saving a large amount of time and money as small-scale conventional machining and manufacturing can be around 80% of the total manufacturing cost for a new product (48). AM removing or reducing the need for costly machining will significantly lower this percentage even while creating more complex geometries than ever before. Essentially, AM holds the key for quicker and cheaper creation of unprecedented geometries over conventional manufacturing. Additionally, binder-jetting for example, a subset of AM 3D Printing, is easily scalable by simply multiplying the size of the operation (49). Due to AM’s attractive nature, the ceramics industry has realized many applications in a diversity of fields.

Specifically, ceramic binder-jet additive manufacturing has been implemented to create parts for a variety of biomedical and aerospace projects. Biomedical studies produced from various bio-ceramics groups indicate a large potential of AM bone repair scaffolds for in vivo implementation for a plethora of ailments (50–52). In the aerospace industry, studies for engine applications of ceramic binder-jetting shows promise for creating fully non-metallic gas turbine engines with carbide-based CMCs (53). These investigations also present successful examples of UHTC additive manufacturing of materials, such as tungsten carbide (54). These overwhelming positive examples of creation and implementation of AM ceramics with binder-jetting are extremely useful when looking towards future, novel applications of these materials.

9 Binder-Jet Additive Manufacturing of Ceramics

For Gen3 CSP HEX manufacturing based on TPMS geometries with extremely complex structures of ceramic, AM with binder-jetting could potentially meet the requirements necessary. Conventional machining technologies simply are unable to produce TPMS geometries with internal volumes. AM's unprecedented nature and proven successes exemplify the promise for implementation for this application.

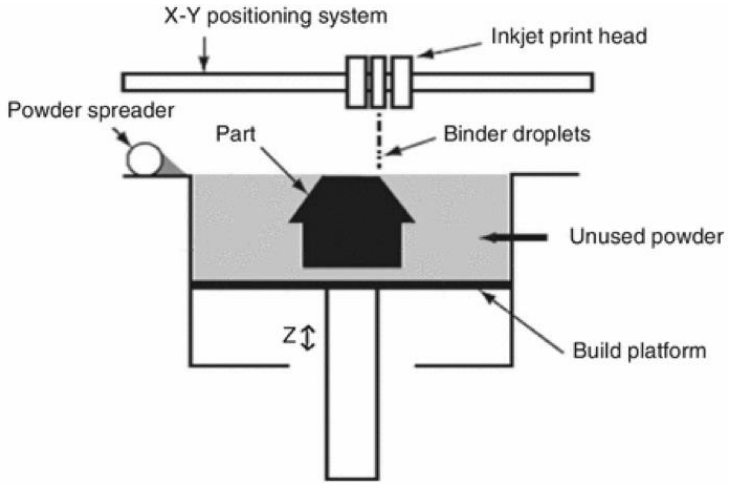

Figure 11. Schematic of binder-jet equipment. (55)

One of the many subsets of additive manufacturing is 3D printing, which then further splits into two groups: direct and indirect printing. Binder-jetting is an indirect printing technique. Its process consists of three main steps, first, the powder is spread across the printing bed surface by the powder spreader in fig.11. Second, in a layer-specific pattern, the inkjet print heads spray binder over the powder surface. Third, the printing bed is slightly lowered along the z axis to make room for the next layer. These three steps are repeated many times until the desired product is entirely built. Where the binder is sprayed, the powder forms a single layer of the product. During the build, the product is fully supported by the surrounding excess powder in the bed; thus, structural supports are not necessary. After the binder-jet process the excess powder is removed around and within the product. For product materials such as sand casting molds, this is the final step. For ceramics, densification, a type of post-processing is required to reach the final desired density through pressureless sintering or other methods (56). Relative to conventional manufacturing and its need for a variety of tools and techniques based on shape, material, etc., binder-jet AM is an extremely simple way to create various geometries using all different materials using only one machine and the same 3 main steps.

9.1 Five Key Factors

Lv et al. defines five key factors of any binder-jet process: powders, binders, printing parameters, equipment, and post-treatment. Defining properties of each key factor is essential to specify a binder-jet process. The factors and their respective parameters are essential for reaching desired strength, accuracy, resolution, density, and roughness of a product (56). Additionally, technical gaps and challenges exist within all key factors of binder-jet printing.

9.1.1 Powders

Powder parameters include particles' shape, size, and distribution. Additives within the powder are also important to consider. The technical gap with powders lies within its lack of advanced milling processing specifically focused for binder-jetting. This would lead to a powder with minimal variability of its parameters, decreasing inconsistencies between products.

9.1.2 Binders

Binders are defined by their method of binding, the mechanism behind the droplet formation, and the kinetics of its infiltration. Challenges with the binder include weak processed geometries due to low binding forces between the binder and powder. However, a technical gap for this problem is to investigate the effects of adding an initiator to the binder for a stronger crosslink between the two.

9.1.3 Printing Parameters

The printing parameters factor is essentially the machine settings to precisely bind the powder. This includes layer thickness, volume fraction of solid binder, orientation of printing, and the binder saturation of each layer. The effect that these parameters have on the final product is not concretely understood and requires computer simulations and further investigation.

9.1.4 Equipment

The binder-jet equipment's functioning capabilities and condition also plays a significant role. This directly effects every layer of the build and can limit the performance of parts. However, this can be seen in the 3D printing industry as increased interest has led to recent unprecedented advancements in the equipment, thus showing promise for binder-jet printing.

9.1.5 Post-Processing

Lastly, post-processing technically is not a part of the binder-jet process but is essential to consider when reach the final state of some ceramic parts. This includes powder removal and further densification. This determines the outcome density of the part, and with further investigation can expand ceramic AM part's potential applications.

By adjusting the properties of the 5 key factors of powder, binder, printing parameters, equipment, and post-treatment, the strength, accuracy, resolution, density, and roughness can be manipulated to meet the desired physical and mechanical characteristics.

10 References

1. Mehos M, Turchi C, Vidal J. Concentrating Solar Power Gen3 Demonstration Roadmap. Golden, Colorado: National Renewable Energy Laboratory; 2017 Jan. Report No.: NREL/TP-5500-67464.

2. SETO Multi-Year Program Plan [Internet]. Solar Energy Technologies Office; 2018 Feb. Report No.: DOE/EE-1739. Available from: https://www.energy.gov/sites/prod/files/2018/02/f48/2018%20SETO%20Portfolio%20Book.pdf

3. Turchi CS, Ma Z, Neises TW, Wagner MJ. Thermodynamic Study of Advanced Supercritical Carbon Dioxide Power Cycles for Concentrating Solar Power Systems. Journal of Solar Energy Engineering. 2013 Nov 1;135(4):041007.

4. Standards of Tubular Heat Exchangers Manufacturers Association. 10th ed. Tarrytown, New York: Tubular Exchanger Manufacturers Association; 2019.

5. Shell and tube heat exchanger [Internet]. Forain.net. Available from: https://www.forain.net/news/shell-and-tube-heat-exchanger

6. Heat Transfer by Plate Heat Exchangers [Internet]. EWP. Available from: http://www.wermac.org/equipment/plateheatexchanger.html

7. Shah R, Sekulić D. Heat Exchangers. In: Handbook of Heat Transfer. 3rd ed. New York, New York: McGraw, Hill; 1998.

8. Paikert P. Air-Cooled Heat Exchangers. In: Heat Exchanger Design Handbook. Washington, DC: Hemisphere; 1982.

9. Alfa Laval Air Cooler: Olmi-Working Principle [Internet]. Alfalaval.com. Available from: https://www.alfalaval.com/products/heat-transfer/finned-tube-air-heat-exchangers/finned-tube-air-heat-exchangers/finned-tube-air-heat-exchangers/

10. Kapfer SC, Hyde ST, Mecke K, Arns CH, Schröder-Turk GE. Minimal surface scaffold designs for tissue engineering. Biomaterials. 2011 Oct;32(29):6875–82.

11. Maskery I, Sturm L, Aremu AO, Panesar A, Williams CB, Tuck CJ, et al. Insights into the mechanical properties of several triply periodic minimal surface lattice structures made by polymer additive manufacturing. Polymer. 2018 Sep;152:62–71.

12. Yang X, Yu H, Wang R, Fane AG. Optimization of microstructured hollow fiber design for membrane distillation applications using CFD modeling. Journal of Membrane Science. 2012 Dec;421–422:258–70.

13. Çulfaz PZ, Buetehorn S, Utiu L, Kueppers M, Bluemich B, Melin T, et al. Fouling Behavior of Microstructured Hollow Fiber Membranes in Dead-End Filtrations: Critical Flux Determination and NMR Imaging of Particle Deposition. Langmuir. 2011 Mar;27(5):1643–52.

14. Çulfaz PZ, Wessling M, Lammertink RGH. Hollow fiber ultrafiltration membranes with microstructured inner skin. Journal of Membrane Science. 2011 Mar;369(1–2):221–7.

15. Ghogomu JN, Guigui C, Rouch JC, Clifton MJ, Aptel P. Hollow-fibre membrane module design: comparison of different curved geometries with Dean vortices. Journal of Membrane Science. 2001 Jan;181(1):71–80.

16. Kaufhold D, Kopf F, Wolff C, Beutel S, Hilterhaus L, Hoffmann M, et al. Generation of Dean vortices and enhancement of oxygen transfer rates in membrane contactors for different hollow fiber geometries. Journal of Membrane Science. 2012 Dec;423–424:342–7.

17. Liu S. Preparation of coiled hollow-fiber membrane and mass transfer performance in membrane extraction. Journal of Membrane Science. 2003 Apr 15;215(1–2):203–11.

18. Jani JM, Wessling M, Lammertink RGH. Geometrical influence on mixing in helical porous membrane microcontactors. Journal of Membrane Science. 2011 Aug;378(1–2):351–8.

19. Jie L, Liu L, Yang F, Liu F, Liu Z. The configuration and application of helical membrane modules in MBR. Journal of Membrane Science. 2012 Mar;392–393:112–21.

20. Kuakuvi DN, Moulin P, Charbit F. Dean vortices: a comparison of woven versus helical and straight hollow fiber membrane modules. Journal of Membrane Science. 2000 Jun;171(1):59–65.

21. Moll R, Veyret D, Charbit F, Moulin P. Dean vortices applied to membrane process. Journal of Membrane Science. 2007 Feb;288(1–2):307–20.

22. Borneman Z, Groothuis B, Willemsen M, Wessling M. Coiled fiber membrane chromatography. Journal of Membrane Science. 2010 Jan;346(2):327–34.

23. Femmer T, Kuehne AJC, Wessling M. Estimation of the structure dependent performance of 3-D rapid prototyped membranes. Chemical Engineering Journal. 2015 Aug;273:438–45.

24. Lord E, Mackay A. Periodic Minimal Surfaces of Cubic Symmetry. Current Science. 2003;85:346–62.

25. Schoen AH. Infinite Periodic Minimal Surfaces without Self-Intersections. Cambridge, Massachusetts: Electronics Research Center; 1970 May. Report No.: NASA TN D-5541.

26. Richlen S. A Survey of Ceramic Heat Exchanger Opportunities. In: Ceramics in Heat Exchangers. Columbus, Ohio: American Ceramic Society; 1985. p. 3–14. (Advances in ceramics).

27. Sommers A, Wang Q, Han X, T'Joen C, Park Y, Jacobi A. Ceramics and ceramic matrix composites for heat exchangers in advanced thermal systems—A review. Applied Thermal Engineering. 2010 Aug;30(11–12):1277–91.

28. Gürdal Z, Haftka RT, Hajela P. Mechanics of Laminated Composite Materials. In: Design and optimization of laminated composite materials. New York, NY: Wiley; 1999. (A Wiley-Interscience Publication).

29. Smyth R. The use of high temperature heat exchangers to increase power plant thermal efficiency. In Honolulu, HI, USA: IEEE; 1997 [cited 2020 Aug 23]. p. 1690–5. Available from: http://ieeexplore.ieee.org/document/656676/

30. Caccia M, Tabandeh-Khorshid M, Itskos G, Strayer AR, Caldwell AS, Pidaparti S, et al. Ceramic–metal composites for heat exchangers in concentrated solar power plants. Nature. 2018 Oct;562(7727):406–9.

31. Haunstetter J, Dreißigacker V, Zunft S. Ceramic high temperature plate fin heat exchanger: Experimental investigation under high temperatures and pressures. Applied Thermal Engineering. 2019 Mar;151:364–72.

32. Jaffe H. Development and testing of superior nozzle materials. Washington, DC: National Aeronautics and Space Administration; 1961 Apr. Report No.: NASw-67.

33. Freeman JW, Cross H. Notes on Heat-Resistant Materials in Britain from technical mission October 13 to November 30, 1950 [Internet]. Washington, DC: National Advisory Committee for Aeronautics; 1051 May. Report No.: NACA RM 51D23. Available from: http://naca.central.cranfield.ac.uk/reports/1951/naca-rm-51d23.pdf

34. Joint Conference on Lifting Manned Hypervelocity and Reentry Vehicles: A Compilation of the Papers Presented [Internet]. Langley Field, Virginia: U.S. Air Force National Aeronautics and Space Administration; 1960 Apr. Report No.: NASA-TMX-67563. Available from: https://ntrs.nasa.gov/citations/19720063091

35. Thermal Protection Systems: Report on the Aspects of Thermal Protection of Interest to NASA and the Related Materials R & D Requirements [Internet]. Washington, DC: National Aeronautics and Space Administration; 1962 Feb. Report No.: NASA-TM-X-650. Available from: https://ntrs.nasa.gov/citations/19660024062

36. Rasky D, Bull J. Ulta-High Temperature Ceramics [Internet]. Moffett Field, CA: NASA Ames Research Center; 1994 May. Report No.: NASA Project: RTOP 232-01-04. Available from: https://ntrs.nasa.gov/citations/20010114148

37. Fahrenholtz WG. A Historical Perspective on Research Related to Ultra-High Temperature Ceramics. In: Fahrenholtz WG, Wuchina EJ, Lee WE, Zhou Y, editors. Ultra-High Temperature Ceramics [Internet]. Hoboken, NJ: John Wiley & Sons, Inc; 2014 [cited 2020 Aug 21]. p. 6–32. Available from: http://doi.wiley.com/10.1002/9781118700853.ch2

38. NASA Armstrong Fact Sheet: Space Shuttles [Internet]. NASA.gov. Available from: https://www.nasa.gov/centers/armstrong/news/FactSheets/FS-015-DFRC.html

39. Wu Y-D, Zhang G-H, Wang Y, Xu R. Low-Temperature Synthesis of VB2 Nanopowders by a Molten-Salt-Assisted Borothermal Reduction Process. Metall and Materi Trans B. 2019 Aug;50(4):1696–703.

40. Song Q, Zhang Z, Xie H, Yin H, Ning Z. Carbonization of transition metals in molten salts. Phys Chem Chem Phys. 2019;21(32):17801–10.

41. Liu H, Deng C, Wang X, Yu C, Ding J, Zhu H. Low-temperature synthesis and properties of VN nanopowder via a combined molten salt nitridation and magnesium thermal reduction. Ceramics International. 2019 Sep;45(13):16638–44.

42. Ma J, Gu Y, Shi L, Chen L, Yang Z, Qian Y. Synthesis and thermal stability of nano-crystalline vanadium disilicide. Journal of Alloys and Compounds. 2004 May;370(1–2):281–4.

43. Li Y, Wu H, Kim H-N, Liu X, Huang Z. Simultaneously enhanced toughness and strain tolerance of SiC-based ceramic composite by in-situ formation of VB2 particles. Journal of the European Ceramic Society. 2017 Jan;37(1):399–405.

44. Gubernat A. Pressureless sintering of single-phase tantalum carbide and niobium carbide. Journal of the European Ceramic Society. 2013 Nov;33(13–14):2391–8.

45. Ran S, Gao L. Spark Plasma Sintering of Nanocrystalline Niobium Nitride Powders. J American Ceramic Society. 2008 Feb;91(2):599–602.

46. Chen Z, Yan Y. Fabrication and microstructure evolution of niobium-niobium silicide composites by spark plasma sintering. J Wuhan Univ Technol. 2007 Jun;22(2):299–302.

47. Additive Manufacturing Overview [Internet]. ASTM International. 2020. Available from: https://www.astm.org/industry/additive-manufacturing-overview.html

48. Klocke F. Modern approaches for the production of ceramic components. Journal of the European Ceramic Society. 1997 Jan;17(2–3):457–65.

49. A. Zocca. LSD-based 3D printing of alumina ceramics. J Ceram Sci Tech [Internet]. 2017 [cited 2020 Aug 21];(01). Available from: http://doi.org/10.4416/JCST2016-00103

50. Fierz FC, Beckmann F, Huser M, Irsen SH, Leukers B, Witte F, et al. The morphology of anisotropic 3D-printed hydroxyapatite scaffolds. Biomaterials. 2008 Oct;29(28):3799–806.

51. Butscher A, Bohner M, Roth C, Ernstberger A, Heuberger R, Doebelin N, et al. Printability of calcium phosphate powders for three-dimensional printing of tissue engineering scaffolds. Acta Biomaterialia. 2012 Jan;8(1):373–85.

52. Seitz H, Rieder W, Irsen S, Leukers B, Tille C. Three-dimensional printing of porous ceramic scaffolds for bone tissue engineering. J Biomed Mater Res. 2005 Aug;74B(2):782–8.

53. Singh M, Halbig MC, Grady JE. Additive Manufacturing of Light Weight Ceramic Matrix Composites For Gas Turbine Engine Applications. In: Ohji T, Singh M, Halbig M, editors. Ceramic Engineering and Science Proceedings [Internet]. Hoboken, NJ, USA: John Wiley & Sons, Inc.; 2015 [cited 2020 Aug 21]. p. 145–50. Available from: http://doi.wiley.com/10.1002/9781119211662.ch16

54. Cramer CL, Nandwana P, Lowden RA, Elliott AM. Infiltration studies of additive manufacture of WC with Co using binder jetting and pressureless melt method. Additive Manufacturing. 2019 Aug;28:333–43.

55. Gibson I, Rosen DW, Stucker B. Additive Manufacturing Technologies [Internet]. Boston, MA: Springer US; 2010 [cited 2020 Aug 23]. Available from: http://link.springer.com/10.1007/978-1-4419-1120-9

56. Lv X, Ye F, Cheng L, Fan S, Liu Y. Binder jetting of ceramics: Powders, binders, printing parameters, equipment, and post-treatment. Ceramics International. 2019 Jul;45(10):12609–24.